

Lattice Boltzmann model for collisionless electrostatic drift wave turbulence obeying Charney-Hasegawa-Mima dynamics

M. Held^{1, a)} and A. Kendl^{1, b)}

*Institute for Ion Physics and Applied Physics, Association Euratom-ÖAW,
University of Innsbruck, A-6020 Innsbruck, Austria*

A lattice Boltzmann method (LBM) approach to the Charney-Hasegawa-Mima (CHM) model for adiabatic drift wave turbulence in magnetised plasmas, is implemented. The CHM-LBM model contains a barotropic equation of state for the potential, a force term including a cross-product analogous to the Coriolis force in quasigeostrophic models, and a density gradient source term. Expansion of the resulting lattice Boltzmann model equations leads to cold-ion fluid continuity and momentum equations, which resemble CHM dynamics under drift ordering. The resulting numerical solutions of standard test cases (monopole propagation, stable drift modes and decaying turbulence) are compared to results obtained by a conventional finite difference scheme that directly discretizes the CHM equation. The LB scheme resembles characteristic CHM dynamics apart from an additional shear in the density gradient direction. The occurring shear reduces with the drift ratio and is ascribed to the compressible limit of the underlying LBM.

^{a)}Electronic mail: markus.held@uibk.ac.at

^{b)}Electronic mail: alexander.kendl@uibk.ac.at

I. INTRODUCTION

The lattice Boltzmann method (LBM) has been established as a promising tool for computations in fluid dynamics, including turbulence, reactive and complex flows. The LB method to model fluid partial differential equations in the framework of a reduced discrete kinetic theory has also been applied to plasma physics. Problems like magnetohydrodynamic turbulence (treated for example in refs.^{1–14}), magnetic reconnection^{15–17}, and a first approach to electrostatic turbulence¹⁸ have been addressed in this framework.

The Charney-Hasegawa-Mima (CHM) equation serves as a basic prototypical two-dimensional one-field model for collisionless electrostatic drift wave turbulence in magnetised plasmas with cold ions and isothermal electrons with an adiabatic response. Drift wave turbulence taps free energy from the background plasma pressure gradient to drive advective nonlinear motion of pressure disturbances by the $E \times B$ drift velocity perpendicular to the magnetic field \mathbf{B} . Parallel dynamics are captured by the electron currents which are balancing the pressure deviations electrostatically with an adiabatic response along the magnetic field. The spatial scale is highly anisotropic permitting us to decouple the parallel dynamics from the perpendicular drift plane motion obeying the two-dimensional (normalized) CHM equation^{19,20}

$$\left(1 - \nabla^2\right) \frac{\partial \delta\phi}{\partial t} + \frac{\partial \delta\phi}{\partial y} - \left\{ \delta\phi, \nabla^2 \delta\phi \right\} = 0 \quad (1)$$

where the advective nonlinearity is expressed by a Poisson bracket $\{A, B\} = \partial_x A \partial_y B - \partial_y A \partial_x B$. The equation is normalized according to $\mathbf{x} \leftarrow \mathbf{x}/\rho_s$ and $t \leftarrow \kappa_n \omega_{ci} t$ for the length and time scales and fluctuations $\delta\phi \leftarrow \kappa_n^{-1}(e\phi/T_e)$ for the electrostatic potential ϕ . These scales represent the dominant contributions to turbulent transport in magnetised plasmas, where the drift frequency $\omega \sim (\rho_s/L_n) \omega_{ci}$ appears to be lower in magnitude than the ion gyro frequency $\omega_{ci} = c_s/\rho_s$ describing the gyro-motion of ions around the magnetic field lines. The magnitude is specified by the ratio of the drift scale $\rho_s = \sqrt{m_i T_e}/eB$ (corresponding to a gyro radius of ions of mass m_i at electron temperature T_e) to the gradient length $L_n = |\partial_x \ln n_0(x)|^{-1}$ of the static background density $n_0(x)$ and is typically defined by the drift ratio $\kappa_n = \rho_s/L_n \ll 1$. The sound speed $c_s = \sqrt{T_e/m_i}$ is given in terms of the electron temperature and ion mass. Finite ion temperature ($T_i > 0$) effects arise when the ion gyro-radius $\rho_i = \sqrt{m_i T_i}/eB$ approaches typical fluctuation scales and are beyond the scope of the model. More detailed gyrokinetic or gyrofluid models put emphasize on

accurate averaging procedures over gyro-motion and modifications to the polarization equation^{21–23}.

The CHM equation can be either obtained from a gyrokinetic model, or from the continuity and momentum equations for a cold uniformly magnetised ion fluid ($T_i \ll T_e$) with adiabatic electron response and a negative background density gradient in x-direction, $n_i = n_e = n_0(x) \exp[e\phi/kT_e]$. The normalized ion continuity and momentum equations can be expressed in terms of the potential instead of density²⁴ as

$$\kappa_n \frac{d}{dt} \delta\phi + \nabla \cdot \mathbf{u} = \kappa_n \mathbf{u} \cdot \nabla x \quad (2)$$

$$\kappa_n \frac{d}{dt} \mathbf{u} + \mathbf{e}_z \times \mathbf{u} = -\nabla \delta\phi \quad (3)$$

where $d/dt = \partial_t + \mathbf{u} \cdot \nabla$ is the advective derivative. Expanding $\delta\phi$ and \mathbf{u} in an asymptotic series with the drift ratio $\kappa_n \ll 1$ as small expansion parameter and accordant ordering²⁴ yields the CHM eq. (1). Replacing the drift ratio κ_n with the Rossby number Ro and identifying the electrostatic potential fluctuations with the dimensionless surface height reveals the isomorphism to the quasi-geostrophic single layer shallow water equations in the β -plane approximation. By replacing the density gradient with a bottom topography or a spatially varying Coriolis frequency the CHM equation is resembled in the limit of a small Rossby number $Ro \ll 1$. Advances with the Lattice Boltzmann method to the shallow water equations have been made by Zhong et al.^{25–27} and Dellar²⁸.

II. LATTICE BOLTZMANN MODEL

A. Boltzmann equation

Starting point for the lattice discretization is the Boltzmann equation for the kinetic distribution function $f(\mathbf{x}, \boldsymbol{\xi}, t)$ with a Bhatnagar-Gross-Krook (BGK) collision operator $C = -(f - f^{eq})/\tau_c$, which expresses the relaxation to a local Maxwellian for a time constant τ_c . Applying the diffusive scaling $t \rightarrow t/\epsilon^2$ and $\mathbf{x} \rightarrow \mathbf{x}/\epsilon$ on the Boltzmann equation results in its dimensionless form²⁹

$$\frac{\partial}{\partial t} f + \frac{1}{\epsilon} \boldsymbol{\xi} \cdot \nabla f = \frac{1}{\epsilon^2} [A(f - f^{eq}) + F], \quad (4)$$

where source and force terms are included in a forcing function as $F(\mathbf{x}, \boldsymbol{\xi}, t) = -\mathbf{a} \cdot \nabla_{\boldsymbol{\xi}} f(\mathbf{x}, \boldsymbol{\xi}, t) + s(\mathbf{x}, \boldsymbol{\xi}, t)$ and the single time collision operator is defined by $A = -1/(\epsilon\tau)$

The Knudsen number $\epsilon = \lambda_m/L_0$ and the non-dimensional relaxation time $\tau = \tau_c/t_c$ are here defined in relation to characteristic drift scale $L_0 = \rho_s$ and to the collision time $t_c = \lambda_m/U_0$ with mean free path length $\lambda_m = e_m\tau_c$ and characteristic (drift) velocity $U_0 = \kappa_n c_s$. The dimensionless relaxation time $\tau = U_0/e_m$ relates the flow velocity to the (lattice) molecular velocity e_m whereas the Mach number $Ma = U_0/c_s$ is identified with the drift parameter κ_n .

The dynamics in the fluid limit, given by eqs. (2) and (3), can be consistently described with the kinetic eq. (4) assuming a local Maxwellian equilibrium distribution function of the form⁶

$$f^{eq} = \frac{\phi}{(2\pi\Theta)^{D/2}} \exp\left[-\frac{(\boldsymbol{\xi} - \mathbf{u})^2}{2\Theta}\right]. \quad (5)$$

The squared dimensionless barotropic speed of sound $\Theta = \phi/(2\kappa_n^2)$ results from the barotropic pressure term $P = \phi^2/(2\kappa_n^2)$ appearing on the macroscopic level as in eq. (3). The isothermal squared speed of sound is defined by $\theta = 1/\kappa_n^2$.

Macroscopic quantities are defined by taking velocity moments over the distribution function

$$\phi = \int f d\boldsymbol{\xi} \quad (6)$$

$$\phi \mathbf{u} = \int \boldsymbol{\xi} f d\boldsymbol{\xi} \quad (7)$$

$$\boldsymbol{\Pi}^{(0)} = \int \boldsymbol{\xi} \boldsymbol{\xi} f^{eq} d\boldsymbol{\xi} = P \mathbf{I} + \phi \mathbf{u} \mathbf{u} \quad (8)$$

and over the forcing function

$$\int F d\boldsymbol{\xi} = \phi s \quad (9)$$

$$\int \boldsymbol{\xi} F d\boldsymbol{\xi} = \phi \mathbf{a} \quad (10)$$

$$\int \boldsymbol{\xi} \boldsymbol{\xi} F d\boldsymbol{\xi} = \phi(\mathbf{a} \mathbf{u} + \mathbf{u} \mathbf{a}) + \phi \frac{dP}{d\phi} s \mathbf{I}. \quad (11)$$

B. Lattice Boltzmann equation

The discretization of the continuum velocity space to 9 directions in 2 dimensions (D2Q9) casts the set of velocities to $\{\boldsymbol{\xi}_0, \boldsymbol{\xi}_1, \dots, \boldsymbol{\xi}_8\}$ and the distribution function and forcing function to $f(\mathbf{x}, \boldsymbol{\xi}_i, t)/w(\boldsymbol{\xi}_i) = f_i(\mathbf{x}, t)/w_i$ and $F(\mathbf{x}, \boldsymbol{\xi}_i, t)/w(\boldsymbol{\xi}_i) = F_i(\mathbf{x}, t)/w_i$ for $i \in (0, \dots, 8)$ with

the continous weight function $w(\boldsymbol{\xi}_i)$ of the Gauss-Hermite quadrature formula. The lattice velocities in D2Q9 geometry are

$$\boldsymbol{\xi}_0 = (0, 0) \quad (12)$$

$$\boldsymbol{\xi}_i = \sqrt{3} \xi_m (\cos \alpha_i, \sin \alpha_i) \quad \text{for } i = 1, 2, 3, 4 \quad (13)$$

$$\boldsymbol{\xi}_i = \sqrt{6} \xi_m (\cos \beta_i, \sin \beta_i) \quad \text{for } i = 5, 6, 7, 8 \quad (14)$$

where $\alpha_i = (i - 1)\pi/2$ and $\beta_i = \alpha_i + \pi/4$. The lattice speed of sound is defined by $\xi_m = (1/\sqrt{3})(\delta x/\delta t)$ with lattice grid size $\delta x = L_B/N_x$ and time step δt . The numerical box size L_B with N_x grid points per space dimension crucially determines whether the CHM is resolved in the drift wave limit.

The choice of the correct equilibrium distribution function for a LBM depends mainly on the equation of state and the lattice geometry. The equilibrium distribution function for a barotropic equation of state acting on a D2Q9 lattice has been determined by Dellar⁶ who showed that an augmentation of the hydrodynamic equilibrium distribution function by ghost modes is leading to a stable scheme if the ghost variables are properly set.

The equilibrium distribution function from ref.⁶ equals one previously derived from an ansatz Method in ref.³⁰:

$$\begin{aligned} f_0^{eq} &= w_0 \phi \left[\frac{9}{4} - \frac{5}{4} \frac{P(\phi)}{\phi \theta} - \frac{\mathbf{u}^2}{2\theta} \right] \\ f_i^{eq} &= w_i \phi \left[\frac{P(\phi)}{\phi \theta} + \frac{\boldsymbol{\xi}_i \cdot \mathbf{u}}{\theta} + \frac{(\boldsymbol{\xi}_i \cdot \mathbf{u})^2}{2\theta^2} - \frac{\mathbf{u}^2}{2\theta} \right]. \end{aligned} \quad (15)$$

Taking the discrete velocity moments

$$\sum_{i=0}^8 f_i^{eq} = \phi \quad (16)$$

$$\sum_{i=0}^8 f_i^{eq} \boldsymbol{\xi}_i = \phi \mathbf{u} \quad (17)$$

$$\sum_{i=0}^8 f_i^{eq} \boldsymbol{\xi}_i \boldsymbol{\xi}_i = \phi \mathbf{u} \mathbf{u} + P \mathbf{I} = \boldsymbol{\Pi}^{(0)} \quad (18)$$

$$\sum_{i=0}^8 f_i^{eq} \xi_{i\alpha} \xi_{i\beta} \xi_{i\gamma} = \theta \phi (u_\alpha \delta_{\beta\gamma} + u_\beta \delta_{\gamma\alpha} + u_\gamma \delta_{\alpha\beta}) = \Lambda_{\alpha\beta\gamma}^{(0)} \quad (19)$$

reveals the deviation to continous kinetic theory where the third velocity moment reads $\Lambda_{\alpha\beta\gamma} = \Theta \phi (u_\alpha \delta_{\beta\gamma} + u_\beta \delta_{\gamma\alpha} + u_\gamma \delta_{\alpha\beta}) + \phi u_\alpha u_\beta u_\gamma$. Hence in the $\Lambda_{\alpha\beta\gamma}^{(0)}$ of the D2Q9 lattice model

the $\mathcal{O}(\epsilon^3)$ triple term is missing and the dimensionless squared isothermal sound speed θ appears instead of the squared barotropic sound speed Θ . These differences are further discussed in A.

The velocity moments over the discrete form of the forcing function determine the force and source terms in the macroscopic equations. The desired fluid system exhibits a velocity dependent force term $\kappa_n^{-1} \mathbf{e}_z \times \mathbf{u}$ containing a cross product and an additional velocity dependent density gradient source term $\kappa_n \mathbf{u} \cdot \nabla x$. The force term is mathematically identical to the Coriolis force, which was already treated by two- and three-dimensional lattice Boltzmann algorithms^{6,25,32,48–50}.

The forcing function proposed in the following resembles the first three velocity moments at the continuum kinetic level, and hence incorporates the barotropic equation of state appearing in the second second velocity moment

$$\sum_{i=0}^8 F_i = \phi s, \quad (20)$$

$$\sum_{i=0}^8 F_i \boldsymbol{\xi}_i = \phi \mathbf{a} \quad (21)$$

$$\sum_{i=0}^8 F_i \boldsymbol{\xi}_i \boldsymbol{\xi}_i = \phi [\mathbf{a} \mathbf{u} + \mathbf{u} \mathbf{a}] + \phi \frac{dP}{d\phi} s \mathbf{I}, \quad (22)$$

The forcing function is derived in an analogous manner to the equilibrium distribution function by considering the ghost variables (see ref.⁶ for details) and generalizes the forcing function of Luo³¹ for complex fluids with a barotropic equation of state.

$$F_i = w_i \phi \left\{ \left[1 + \left(\theta - \frac{dP}{d\phi} \right) \left(\frac{4 + g_i}{4\theta} - \frac{\boldsymbol{\xi}_i^2}{2\theta^2} \right) \right] s + \left[\frac{(\boldsymbol{\xi}_i - \mathbf{u})}{\theta} + \frac{(\boldsymbol{\xi}_i \cdot \mathbf{u}) \boldsymbol{\xi}_i}{\theta^2} \right] \cdot \mathbf{a} \right\} \quad (23)$$

The normalized CHM source and force terms are

$$s = \kappa_n \mathbf{u} \cdot \mathbf{e}_x, \quad (24)$$

$$\mathbf{a} = \frac{1}{\kappa_n} (\mathbf{u} \times \mathbf{e}_z) + \mathbf{u} s. \quad (25)$$

The additional contribution of $\mathbf{u} s$ in the force term will cancel a spurious term in the macroscopic momentum equation, which is detailed in the asymptotic analysis in A.

C. CHM-LBM time integration

The diffusively scaled discrete Boltzmann PDE follows from eq. (4)

$$\frac{\partial f_i}{\partial t} + \frac{1}{\epsilon} \boldsymbol{\xi}_i \cdot \nabla f_i = \frac{1}{\epsilon^2} [A(f_i - f_i^{eq}) + F_i], \quad (26)$$

Writing the left hand side as the total derivative $\frac{d}{ds} f_i(\mathbf{x} + \boldsymbol{\xi}_i s/\epsilon, t + s)$ and integrating both sides of eq. (26) from $s = 0$ to $s = \delta t = \epsilon^2$ yields^{32,47}

$$f_i(\mathbf{x}', t') - f_i(\mathbf{x}, t) = \frac{1}{\epsilon^2} \int_0^{\delta t} h_i(\mathbf{x} + \boldsymbol{\xi}_i s/\epsilon, t + s) ds. \quad (27)$$

with the substitution $h_i = A(f_i - f_i^{eq}) + F_i$ for the right hand side of eq. (26). The implicit lattice Boltzmann equation is now obtained by approximating the integral by a second order accurate numerical quadrature scheme. This is ensured by the trapezoidal rule

$$\frac{1}{\epsilon^2} \int_0^{\delta t} h_i(\mathbf{x} + \boldsymbol{\xi}_i s/\epsilon, t + s) ds = \frac{1}{2} [h_i(\mathbf{x}', t') + h_i(\mathbf{x}, t)] + \mathcal{O}(\epsilon^4) \quad (28)$$

with the substitution $(\mathbf{x}', t') = (\mathbf{x} + \boldsymbol{\xi}_i \epsilon, t + \epsilon^2)$. Writing out the integral yields the implicit form of the lattice Boltzmann equation

$$f_i(\mathbf{x}', t') - f_i(\mathbf{x}, t) = \frac{1}{2} A [f_i(\mathbf{x}', t') + f_i(\mathbf{x}, t) - f_i^{eq}(\mathbf{x}', t') - f_i^{eq}(\mathbf{x}, t)] + \frac{1}{2} [F_i(\mathbf{x}', t') + F_i(\mathbf{x}, t)]. \quad (29)$$

To work around this implicit equation the distribution function is transformed to $f \rightarrow \bar{f}$ as

$$\bar{f}_i(\mathbf{x}, t) = f_i(\mathbf{x}, t) - \frac{A}{2} [f_i(\mathbf{x}, t) - f_i^{eq}(\mathbf{x}, t)] - \frac{1}{2} F_i(\mathbf{x}, t) \quad (30)$$

Introducing now the $\bar{A} = A/[1 - 1/(2A)]$ and $\bar{\lambda} = \bar{A}/A$ and applying the transformation $f \rightarrow \bar{f}$ to eq. (29) resembles the usual form of the explicit LB algorithm

$$\bar{f}_i(\mathbf{x}', t') - \bar{f}_i(\mathbf{x}, t) = \bar{A} [\bar{f}_i(\mathbf{x}, t) - f_i^{eq}(\mathbf{x}, t)] + \bar{\lambda} F_i(\mathbf{x}, t), \quad (31)$$

which is the starting point of the asymptotic analysis presented in A. However, this transformation leads to implicit expressions of the velocity moments over the distribution function as

$$\phi = \sum_{i=0}^N \bar{f}_i + \frac{1}{2} \phi s \quad (32)$$

$$\phi \mathbf{u} = \sum_{i=0}^N \boldsymbol{\xi}_i \bar{f}_i + \frac{1}{2} \phi \mathbf{a} \quad (33)$$

$$\left(1 - \frac{A}{2}\right) \boldsymbol{\Pi} = \sum_{i=0}^N \bar{f}_i \boldsymbol{\xi}_i \boldsymbol{\xi}_i - \frac{A}{2} \boldsymbol{\Pi}^{(0)} + \frac{1}{2} \phi (\mathbf{a} \mathbf{u} + \mathbf{u} \mathbf{a}) + \frac{1}{2} \frac{dP}{d\phi} \phi s \quad (34)$$

Depending on the exact form of the force and source terms these equations may not have an analytical solution which is at the same time computationally efficient, and one has to apply Newton's method to this problem. In this particular case the relevant equations

$$\phi = \bar{\phi} + \frac{1}{2} \frac{1}{L_n} \phi (\mathbf{u} \cdot \mathbf{e}_x) \quad (35)$$

$$\mathbf{u} = \frac{\bar{\phi}}{\phi} \bar{\mathbf{u}} - \frac{1}{2} \omega_{ci} (\mathbf{e}_z \times \mathbf{u}) + \frac{1}{2} \frac{1}{L_n} \mathbf{u} (\mathbf{u} \cdot \mathbf{e}_x) \quad (36)$$

with

$$\bar{\phi} = \sum_{i=0}^N \bar{f}_i \quad \text{and} \quad \bar{\phi} \bar{\mathbf{u}} = \sum_{i=0}^N \xi_i \bar{f}_i \quad (37)$$

could not be solved trivially. An approximation which stays within the scope of the model has to be made at this point. It is justified to drop the third term on the right hand side of the relation for the velocity shift eq. (36). By taking the cross product of the approximated expression we obtain $\mathbf{e}_z \times \mathbf{u} = \left[1 - \frac{1}{2} \frac{1}{L_n} (\mathbf{u} \cdot \mathbf{e}_x) \right] \mathbf{e}_z \times \bar{\mathbf{u}} + \frac{1}{2} \mathbf{u} \omega_{ci}$. This simplifies the equations for the shifts to:

$$\phi \leftarrow \frac{\bar{\phi}}{1 - \frac{1}{2} \frac{1}{L_n} \mathbf{u} \cdot \mathbf{e}_x} \quad (38)$$

$$\mathbf{u} \leftarrow \frac{\bar{\mathbf{u}} - \frac{1}{2} \omega_{ci} (\mathbf{e}_z \times \bar{\mathbf{u}})}{1 + \left(\frac{1}{2} \omega_{ci} \right)^2} \left(1 - \frac{1}{2} \frac{1}{L_n} \mathbf{u} \cdot \mathbf{e}_x \right) \quad (39)$$

D. Boundary Conditions

For stability reasons, specularly reflecting boundary conditions are chosen on the east and west boundaries (in “radial” direction in terms of drift wave terminology), whereas the north and south boundaries (in “poloidal” direction) are treated periodically. The rigid walls on east and west are set on the outermost lattice nodes, which corresponds to an on-site reflection of the perpendicular components of \bar{f} . On east the distribution function is flipped according to $\bar{f}_3 \rightarrow \bar{f}_1$, $\bar{f}_6 \rightarrow \bar{f}_5$, $\bar{f}_7 \rightarrow \bar{f}_8$, and vice versa for the west boundary. Applying the boundary condition on \bar{f} instead of f introduces a small vorticity source on the east and west boundaries, which can be circumvented by subtracting out the F_i terms before updating the boundaries. However, this discrepancy had only minor impact on the present numerical results.

E. The CHM-LBM algorithm

The LBM can be advanced in time by a four step algorithm, after an initialization of the macroscopic fields has been carried out by either setting the initial distribution and computing the macroscopic quantities, or by setting the macroscopic initial fields. In the computations presented in section IV the latter initialization has been applied.

The four-step time cycle includes:

1. Update ϕ and \mathbf{u} by eqs. (38) and (39) with the help of eq. (37) as a function of the previous \bar{f}_i and/or the previous ϕ and \mathbf{u} ;
2. Obtain f_i^{eq} from eq. (15) and F_i from eq. (23) as functions of the updated ϕ and \mathbf{u} ;
3. Collide the particles using

$$\bar{f}_i^*(\mathbf{x}, t) = \bar{f}_i(\mathbf{x}, t) + \bar{A} (\bar{f}_i(\mathbf{x}, t) - f_i^{eq}(\mathbf{x}, t)) + \bar{\lambda} F_i(\mathbf{x}, t); \quad (40)$$

4. Stream the particles to the adjacent nodes using

$$\bar{f}_i(\mathbf{x} + \boldsymbol{\xi}_i \delta t, t + \delta t) = \bar{f}_i^*(\mathbf{x}, t); \quad (41)$$

... and return to step (1).

III. CONVENTIONAL FINITE DIFFERENCE SCHEME FOR THE CHM

The proposed LB model is cross-verified with a conventional finite difference scheme which directly solves the CHM fluid eq. (1), including an artificial hyperviscosity.

The employed Arakawa-Karniadakis scheme has first been applied to drift wave turbulence computations by Naulin and Nielsen³⁴, and uses the 3rd-order accurate energy and enstrophy conserving Arakawa spatial discretization³⁵ for the Poisson bracket nonlinearity in combination with 3rd-order “stiffly stable” time-stepping³⁶. The Karniadakis time-stepping scheme is here however reduced down to 2nd-order to achieve the same temporal accuracy as in the present CHM-LBM algorithm. The electrostatic potential $\delta\phi$ is obtained after time stepping by solution of the generalized Poisson Problem $(1 - \nabla^2)\delta\phi = S$ with a half-wave Fourier transform method. The boundary conditions are periodic in y direction and Dirichlet in x direction. In summary the global accuracy of the reduced Arakawa-Karniadakis method equals the CHM-LB method and is of second order.

IV. NUMERICAL TESTS

For all following computations the drift parameter is set to $\kappa_n = 0.05$, the normalized box size is fixed to $L_B = 64$, and the LB viscosity to $\nu = 0.0002$.

A stable LBM setup, which keeps the $\mathcal{O}(\delta t)$ compressibility error as well as the $\mathcal{O}(\delta x^2)$ lattice error at a minimum level restricts their ratio $(\delta t/\delta x^2)$ to a constant. A ratio of $(\delta t/\delta x^2) \approx \mathcal{O}(1)$ performed with best stability especially in the decaying turbulence simulations. Hence the lattice resolution which fullfills this condition for the chosen parameters is $N_x = 2048$. The initial $E \times B$ drift velocity field is calculated with the help of the lowest order momentum balance equation $\mathbf{e}_z \times \mathbf{u} = (\kappa_n)^{-1} \nabla \phi$. This guarantees that the potential field and the velocity field are consistent, and hence initial pressure waves are suppressed. The finite difference scheme (FD) parameters differ from the LBM setup only by the number of grid points $N_x = 512$ and the hyperviscous term of order 8 with viscosity parameter $\nu_8 = 10^{-9}$.

A. Monopole propagation

The first electrostatic drift wave test case follows the evolution of Gaussian monopoles. Within the framework of the CHM model, monopoles for various initial amplitudes A , corresponding to a rotation number $R_E = A/r_0$, exhibit nearly coherent vortex propagation into the diamagnetic (here: y) direction for a large $R_E \gg 1$, or contrarily, dispersive spreading for small $R_E \ll 1$ ^{24,37}.

In the following test cases, the propagation of initial monopoles with $R_E = 0.1$ (Fig. 1), $R_E = 1$ (Fig. 2) and $R_E = 5$ (Fig. 3) is compared between the LB (first row) and FD (second row) schemes at various times of the computation. The LB algorithm closely resembles the monopole dynamics of the CHM equation posed by the FD scheme, except for a small deviation of the vortex amplitudes at later times (compare Fig. 1 at $t = 25$).

B. Dipole drift modons

Solitary dipole drift vortex solutions or modons are, in contrast to Gaussian monopoles, localized stationary solutions to the CHM equations. For Larichev-Reznik modons, the initial potential perturbation of radial extent R is defined as^{24,38}:

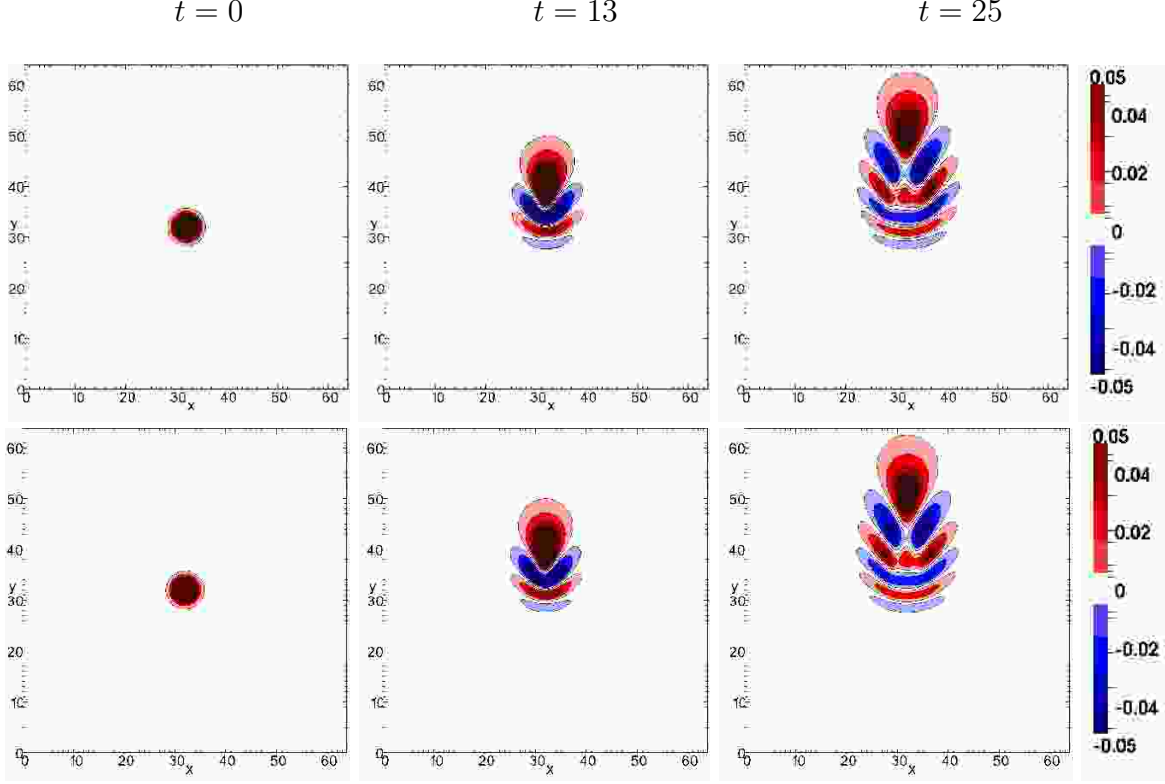


FIG. 1: Evolution of an initial Gaussian monopole for $R_E = 0.1$: the equally spaced isolines represent the potential field $\delta\phi$ of the LBM (first row) and the FD scheme (second row) at various times.

$$\delta\phi(r, \vartheta) = \phi_r(r) \cos(\vartheta) \quad (42)$$

with

$$\phi_r(r) = \begin{cases} u_* r \left(1 + \frac{\beta^2}{\gamma^2}\right) - \frac{u_* R \beta^2 J_1(\gamma r)}{\gamma^2 J_1(\gamma R)} & , r \leq R \\ \frac{u_* R K_1(\beta r)}{K_1(\beta R)} & , r > R \end{cases} \quad (43)$$

where J_1 , J_2 are Bessel functions of the first kind and K_1 , K_2 are modified Bessel functions of the second kind. The parameter $\beta = \sqrt{1 - (u_d/u_*)}$ contains the ratio of the drift velocity u_d to the dipole velocity u_* . The parameter γ is determined by the transcendental equation

$$\frac{K_2(\beta R)}{\beta R K_1(\beta R)} = -\frac{J_2(\gamma R)}{\gamma R K_1(\gamma R)} \quad (44)$$

Its smallest number defines the ground state of the dipole, and higher order solutions are excited states³⁹. The drift modon is stable if the ratio between the typical dipole velocity to the drift velocity fullfills $u_d/u_* \geq 1$ whereas dispersive broadening appears for negative

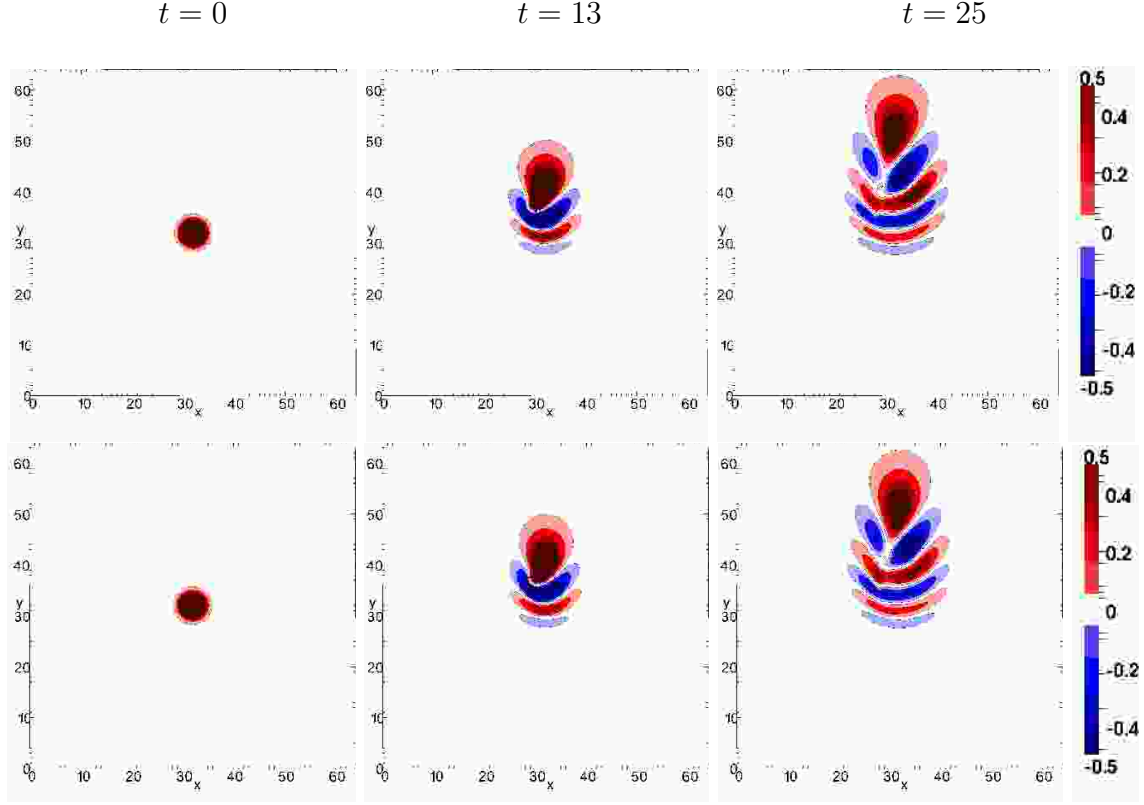


FIG. 2: Evolution of an initial Gaussian monopole for $R_E = 1$: Self focusing is concurring with monopole spreading and results in a mixed form of the linear and nonlinear regime.

ratios. The present computations are restricted to the ground state of stable travelling drift modon with $u_d/u_* = 2$. Fig. 4 shows the expected propagation of the drift modon into the $+y$ direction. For the LB model (first row) an increased shearing of the drift modon is observed in comparison to the classical FD model (second row) with progressing time. In the LB model the lifetime of the stable travelling drift modon is further enhanced by reducing the drift ratio κ_n .

C. Decaying Turbulence

The initial energy spectrum $E_{\delta\phi}(k) \propto k^{30}(k+k_0)^{-60}$ is determined in k -space by a random phase factor and a narrow peak around a wavenumber $k_0^{40,41}$, which is here is fixed to $k_0 = 0.5$. Hence around 32 field modes are initialized into a physical box size of $64\rho_s$. The initial amplitude factor of the electrostatic potential field is chosen that both algorithms remain stable during the computation time, whereby the LBM is more restrictive, and

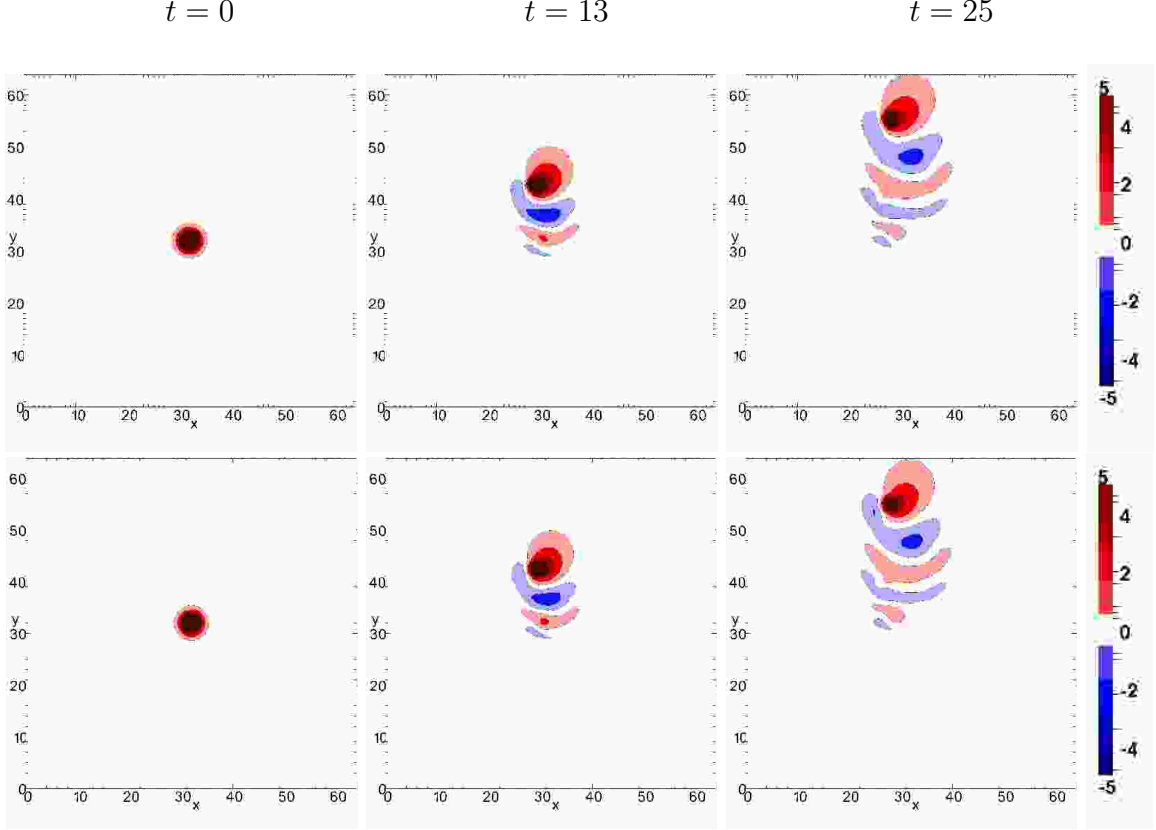


FIG. 3: Evolution of an initial Gaussian monopole for $R_E = 5$: The dominant process is self-focusing, which allows the monopole to propagate nearly dispersionless with the drift velocity. (first row: LBM; second row: FDM)

$\mathcal{O}(\delta\phi) = 0.5$ is used as an exemplary value. This sets the initial values of the total generalized energy and total generalized enstrophy to $\mathcal{E} \approx 0.07$ and $\mathcal{U} \approx 0.7$, which are defined by

$$\mathcal{E} = \frac{1}{N_x N_y} \sum_{i=0}^{N_x-1} \sum_{j=0}^{N_y-1} \frac{1}{2} [\delta\phi^2 + (\nabla\delta\phi)^2], \quad (45)$$

$$\mathcal{U} = \frac{1}{N_x N_y} \sum_{i=0}^{N_x-1} \sum_{j=0}^{N_y-1} \frac{1}{2} [(\nabla\delta\phi)^2 + (\nabla^2\delta\phi)^2]. \quad (46)$$

The spatial gradients are related to the macroscopic velocity via the lowest order momentum balance equation $\mathbf{e}_z \times \mathbf{u} = -\nabla\delta\phi$. Hence the kinetic energy and the enstrophy are derived by $(\nabla\delta\phi)^2 = \mathbf{u}^2$ and $(\nabla^2\delta\phi)^2 = (\partial_x u_y - \partial_y u_x)^2$. The partial derivatives are computed with the help of central differences of second order accuracy. Fig. 5 shows the decaying turbulent potential field. Up to $t \approx 30$ the turbulent field is nearly isotropic. The emerging anisotropy, visible through a pattern of elongated structures into y-direction, gradually increases as the

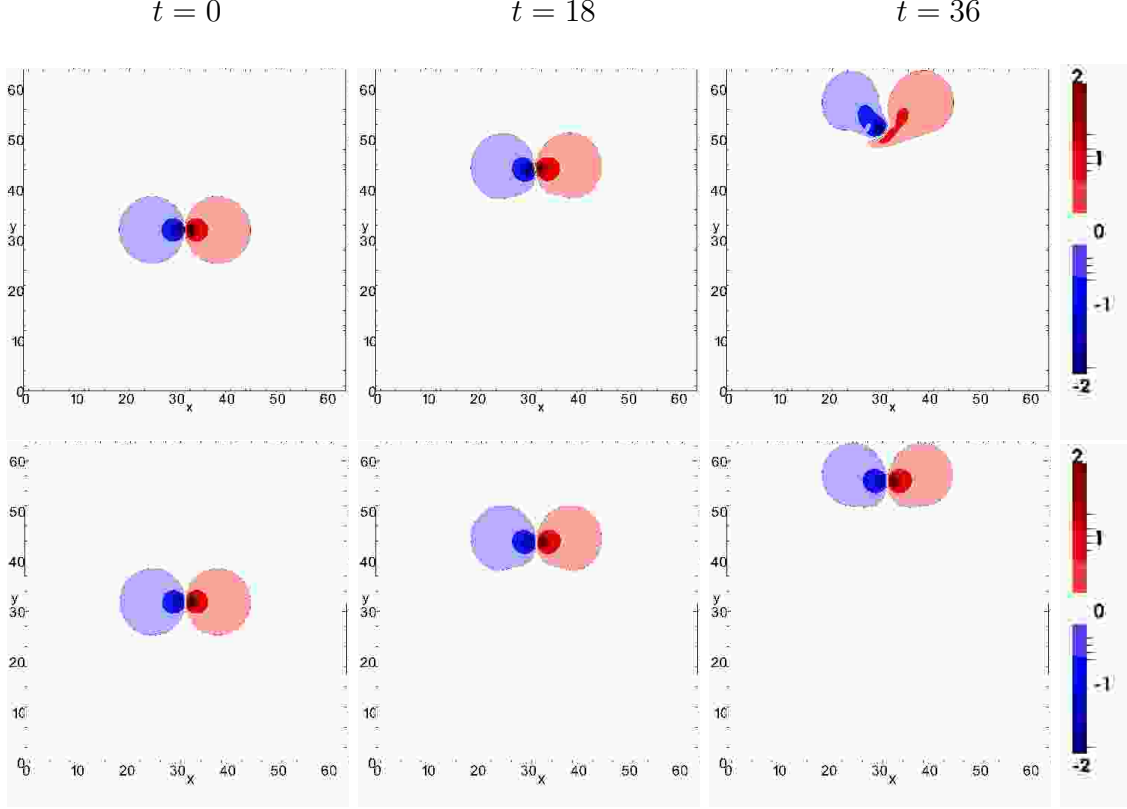


FIG. 4: The potential $\delta\phi$ of a stably propagating drift modon is shown for the LBM (first row) and for the FD scheme (second row). It is clearly visible that for the LBM case the shape of the modon is distorted by a small shear from around $t = 36$ on.

simulation advances. The one-dimensional generalized energy spectra $E(k_x)$ and $E(k_y)$ differ by a few orders of magnitude in the high k_x, k_y range⁴², apart from the dumb-bell shaped two-dimensional generalized energy spectrum (cf.³⁷). The correlation between the turbulent electrostatic potential fields of the LB and FD scheme decreases as time progresses.

Fig. 6 shows the corresponding angle-averaged generalized energy spectrum $E(k)$ of the nearly isotropic state which is defined as the sum over the energy shell within $k \pm \Delta k$:

$$E(k) = \sum_{\mathbf{k}} E(\mathbf{k}), \quad k - \Delta k < |\mathbf{k}| < k + \Delta k \quad (47)$$

$$E(\mathbf{k}) = \frac{1}{2} (|\delta\phi_{\mathbf{k}}|^2 + |\mathbf{k} \delta\phi_{\mathbf{k}}|^2) \quad (48)$$

Due to the non-periodicity of the signal in x -direction a Blackmann-Harris window⁴³ has been used on the Fourier transform. As a result the transformed signals do not alter the overall power law coefficient of the k -spectrum. The obtained power law coefficients resemble

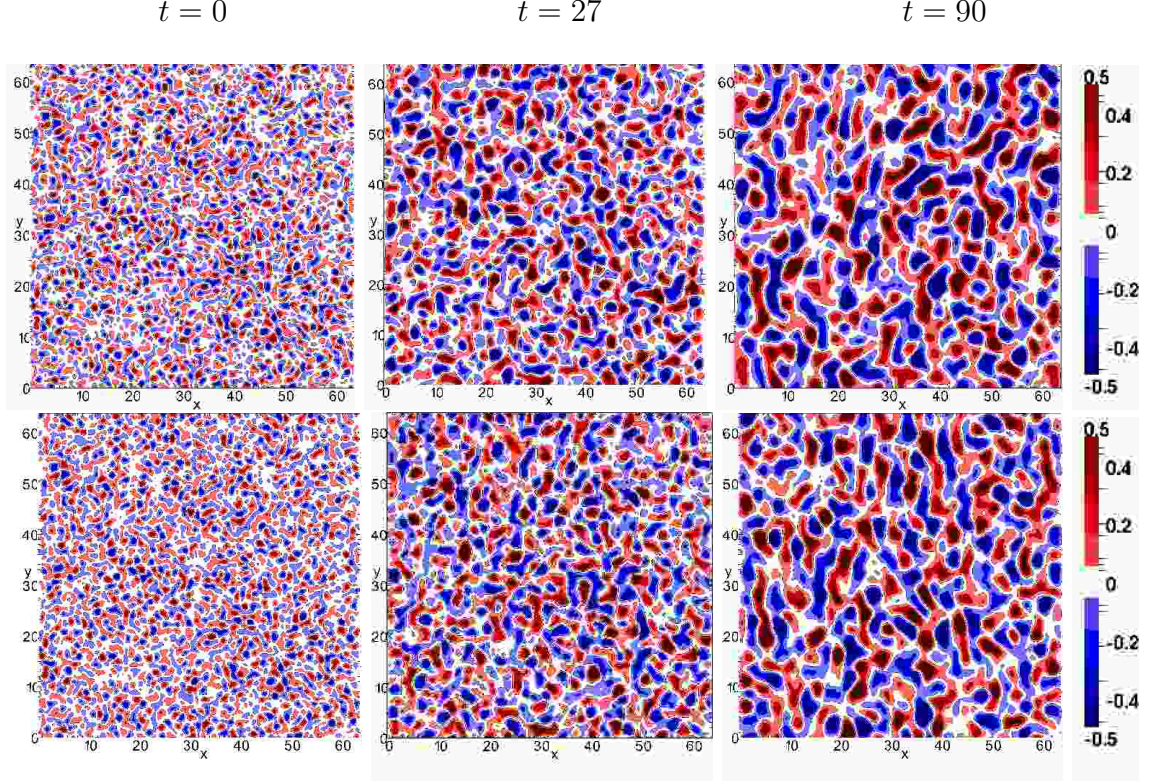


FIG. 5: This electrostatic potential $\delta\phi$ is shown at several times for the FD scheme (first row) and the LBM (second row). The tendency to large scale zonally extended structures is visible in the advanced state ($t = 90$) of the decaying turbulence.

the theoretically⁴⁴ and numerically^{38,40,45} predicted strong turbulence laws

$$E(k) \propto \begin{cases} k^4 & , k < k_{max} \\ k^{-5} & , k_{max} < k \ll 1 \\ k^{-3} & , 1 \ll k \end{cases} \quad (49)$$

except in the high- k dissipative range, where the power law coefficient steepens to approximately k^{-4} . The LBM spectrum moreover reveals a weak peak in the very high k range arising from the residual force term contributions of the free-slip boundary condition.

The time evolution of the generalized energy \mathcal{E} and enstrophy \mathcal{U} for both algorithms are shown in In Fig. 6 the time evolution of the generalized energy \mathcal{E} and enstrophy \mathcal{U} for both algorithms resembles decay power laws. Due to the different treatment of the viscous dissipation the corresponding decay is slower for the hyperviscous implementation in the FD scheme. The deviation at $t = 0$ of the initial variables is based in the differing resolutions

underlying the Fourier transforms of the k -spectra, and in the initialization of the dynamical variables itself. The fitted power law coefficients are of same magnitude as the estimates of $\mathcal{U} \propto t^{-0.5}$ and $\mathcal{E} \propto t^{-0.0540}$.

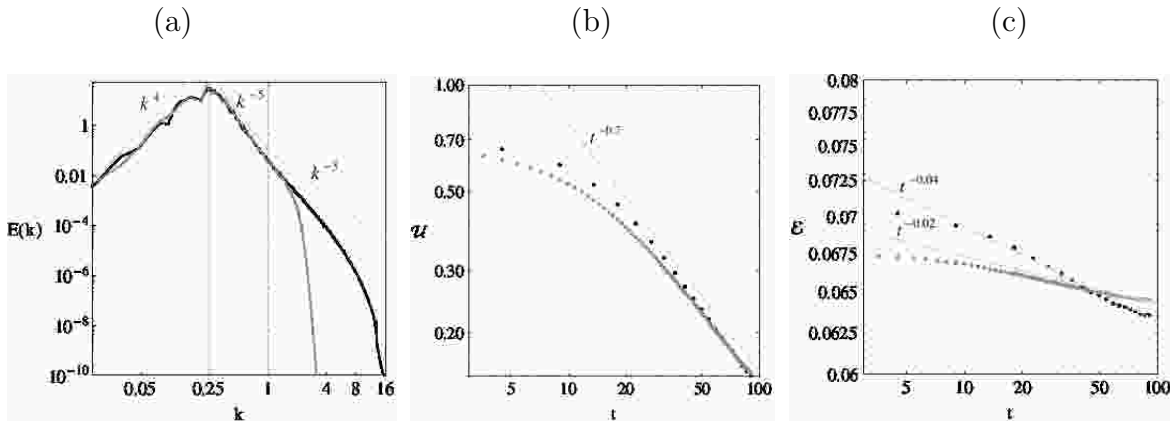


FIG. 6: (a) Double logarithmic plot of the time averaged k -spectrum of the generalized energy $E(k)$. Black line: LBM; gray line: FD. Time averaging was applied between $t = 9$ and $t = 32$. (b) Double logarithmic plot of time evolution of the generalized enstrophy $\mathcal{U}(t)$ for the LBM (black dots) and the FD scheme (gray dots). (c) Double logarithmic plot of time evolution of the generalized energy $\mathcal{E}(t)$ for the LBM (black dots) and the FD scheme (gray dots).

V. CONCLUSION

The presented LBM algorithm for the CHM equation is based on previous single-layer shallow water LBM implementations with an additional source term, which is able to include density gradient effects. Consequently the form of the forcing function is revised to reproduce the correct macroscopic equations in the course of the asymptotic analysis. In order to verify the scheme, computations of decaying turbulence, dipole drift modons and monopole propagation with the new LBM scheme were compared with an established FD scheme.

The numerical results deviate mainly in the observed (in)stability of the drift modon from that of the CHM equation, and resemble apart from that characteristic drift wave turbulence behaviour. The occurring shear in the x -direction reduces with the drift parameter κ_n and persists even if the approximated velocityshifts (eqs. (38) and (39)) are replaced by the

exact expressions. Hence the shear effect is intrinsically related to the compressible limit of the resolved ion continuity and momentum equations.

Alternatively, there is another option to approach the CHM equation via a LB model by replacing the density gradient source term, which appears in the continuity equation with a spatially varying gyro frequency (or Coriolis parameter), by a substitution of $(\mathbf{e}_z \times \mathbf{u}) \rightarrow (1 + \kappa_n x)(\mathbf{e}_z \times \mathbf{u})$ in the momentum equation. As a result the implicit equations comparable with eqs. (38) and (39) yield simple expressions without any further approximations⁴⁶. However, corresponding computations for $\kappa_n = 0.05$ showed a considerable larger shear in the x -direction as the presented LBM algorithm.

ACKNOWLEDGEMENT

This work was partly supported by the Austrian Science Fund (FWF) Y398; by the Austrian Ministry of Science BMWF as part of the UniInfrastrukturprogramm of the Research Platform Scientific Computing at the University of Innsbruck; and by the European Commission under the Contract of Association between EURATOM and ÖAW carried out within the framework of the European Fusion Development Agreement (EFDA). The views and opinions expressed herein do not necessarily reflect those of the European Commission.

Appendix A: Asymptotic analysis

By adopting the diffusive scaling $\delta t \sim \delta x^2 \sim \epsilon^2$ in our LB approach, an asymptotic expansion of the model equations in the spirit of Sone⁵¹, Junk *et al.*^{52,53} and Inamuro *et al.*⁵⁴, will lead directly to an incompressible set of fluid type equations by taking the Mach number and Knudsen number to zero concurrently, while fixing the Reynolds number. Compressibility effects are then related to the diffusive time scale and are understood as numerical artifacts instead of physical effects. In contrast to the Chapman-Enskog (CE) derivation the ordering of the macroscopic variables is not made beforehand, so that the expansion of the macroscopic variables is ambiguous and no further limiting process (e.g. low Mach number) has to be applied to obtain the incompressible fluid equations. To clearly demonstrate the deviations from the incompressible fluid equations up to a specific order in ϵ , we start the derivation from the scaled difference equation (LBE). This is more accurate than just analyz-

ing the discrete Boltzmann PDE and additionally it will alter some terms of the underlying incompressible fluid type equations. We start our analysis from the explicit LB eq. (31), where we expand the distribution function and the forcing function in an asymptotic series of ϵ according to

$$\bar{f}_i(\mathbf{x}, t) = \sum_{m=0}^{\infty} \epsilon^m \bar{f}_i^{(m)}(\mathbf{x}, t), \quad F_i(\mathbf{x}, t) = \sum_{m=0}^{\infty} \epsilon^m F_i^{(m)}(\mathbf{x}, t), \quad (\text{A1})$$

whereby the leading order appears at $\mathcal{O}(\epsilon^3)$ for the forcing function and naturally $F_i^{(0)} = F_i^{(1)} = F_i^{(2)} = 0$. A Taylor approximation of the left-hand side of the LB eq. (31) provides the quantity

$$\bar{f}_i^{(m)}(\mathbf{x}', t') - \bar{f}_i^{(m)}(\mathbf{x}, t) = \sum_{r=0}^{\infty} \epsilon^r D_r(\partial_t, \boldsymbol{\xi}_i \cdot \boldsymbol{\nabla}) \bar{f}_i^{(m)}(\mathbf{x}, t) \quad (\text{A2})$$

with the polynomials given in general by

$$D_r(\partial_t, \boldsymbol{\xi}_i \cdot \boldsymbol{\nabla}) = \sum_{2a+b=r} \frac{(\partial_t)^a (\boldsymbol{\xi}_i \cdot \boldsymbol{\nabla})^b}{a!b!}, \quad r \geq 0 \quad (\text{A3})$$

and practically by

$$D_0(\partial_t, \boldsymbol{\xi}_i \cdot \boldsymbol{\nabla}) = 0, \quad D_1(\partial_t, \boldsymbol{\xi}_i \cdot \boldsymbol{\nabla}) = (\boldsymbol{\xi}_i \cdot \boldsymbol{\nabla}), \quad (\text{A4})$$

$$D_2(\partial_t, \boldsymbol{\xi}_i \cdot \boldsymbol{\nabla}) = \partial_t + (\boldsymbol{\xi}_i \cdot \boldsymbol{\nabla})^2 / 2, \quad D_3(\partial_t, \boldsymbol{\xi}_i \cdot \boldsymbol{\nabla}) = (\boldsymbol{\xi}_i \cdot \boldsymbol{\nabla}) [\partial_t + (\boldsymbol{\xi}_i \cdot \boldsymbol{\nabla})^2 / 6]. \quad (\text{A5})$$

For the sake of convenience the equilibrium distribution function is split into three parts $f_i^{(eq)} = f_i^{(eq,0)} + f_i^{(eq,1)} + f_i^{(eq,2)}$ by analogy with Asinari⁵⁵, whereby the nonvanishing first three moments over the equilibrium distribution functions are given by

$$\sum_{i=0}^8 f_i^{(eq,0)}(\phi^{(k)}) = \phi^{(k)}, \quad \sum_{i=0}^8 \boldsymbol{\xi}_i \boldsymbol{\xi}_i f_i^{(eq,0)}(\phi^{(k)}) = P^{(k)} \mathbf{I}, \quad (\text{A6})$$

$$\sum_{i=0}^8 \boldsymbol{\xi}_i f_i^{(eq,1)}(\phi^{(q)}, \mathbf{u}^{(p)}) = \phi^{(q)} \mathbf{u}^{(p)}, \quad \sum_{i=0}^8 \boldsymbol{\xi}_i \boldsymbol{\xi}_i f_i^{(eq,2)}(\phi^{(q)}, \mathbf{u}^{(p)}, \mathbf{u}^{(r)}) = \phi^{(q)} \mathbf{u}^{(p)} \mathbf{u}^{(r)}. \quad (\text{A7})$$

Combining now the expansions for \bar{f}_i , $f_i^{(eq)}$ and F_i with eq. (31) yields a discrete PDE of order $\mathcal{O}(\epsilon^{k+2})$ with $k \geq 2$

$$\begin{aligned} \partial_t \bar{f}_i^{(k)} + (\boldsymbol{\xi}_i \cdot \boldsymbol{\nabla}) \bar{f}_i^{(k+1)} + \frac{1}{2} (\boldsymbol{\xi}_i \cdot \boldsymbol{\nabla})^2 \bar{f}_i^{(k)} = & \bar{A} \left\{ f_i^{(eq,0)}(\phi^{(k+2)}) + \sum_{p+q=k+2} f_i^{(eq,1)}(\phi^{(q)}, \mathbf{u}^{(p)}) + \right. \\ & \left. \sum_{p+q+r=k+2} f_i^{(eq,2)}(\phi^{(q)}, \mathbf{u}^{(p)}, \mathbf{u}^{(r)}) - \bar{f}_i^{(k+2)} \right\} + L^{(k+2)} \end{aligned} \quad (\text{A8})$$

and the general definition

$$L_i^{(k+2)} = \bar{\lambda} F_i^{(k+2)} - \sum_{\substack{m+r=k+2 \\ m < k}} D_r(\partial_t, \boldsymbol{\xi}_i \cdot \boldsymbol{\nabla}) \bar{f}_i^{(m)}, \quad (\text{A9})$$

revealing differences to an asymptotic analysis of the discrete Boltzmann eq. at $\mathcal{O}(\epsilon^3)$:

$$L_i^{(0)} = L_i^{(1)} = L_i^{(2)} = 0, \quad L_i^{(3)} = \bar{\lambda} F_i^{(3)} - (\boldsymbol{\xi}_i \cdot \boldsymbol{\nabla}) [\partial_t + (\boldsymbol{\xi}_i \cdot \boldsymbol{\nabla})^2 / 6] \bar{f}_i^{(0)}. \quad (\text{A10})$$

Rearranging eq. (A8) to

$$\begin{aligned} \bar{f}_i^{(k+2)} = & f_i^{(eq,0)}(\phi^{(k+2)}) + \sum_{p+q=k+2} f_i^{(eq,1)}(\phi^{(q)}, \mathbf{u}^{(p)}) + \sum_{p+q+r=k+2} f_i^{(eq,2)}(\phi^{(q)}, \mathbf{u}^{(p)}, \mathbf{u}^{(r)}) \\ & - \bar{A}^{-1} \left[\partial_t \bar{f}_i^{(k)} + (\boldsymbol{\xi}_i \cdot \boldsymbol{\nabla}) \bar{f}_i^{(k+1)} + \frac{1}{2} (\boldsymbol{\xi}_i \cdot \boldsymbol{\nabla})^2 \bar{f}_i^{(k)} \right] + \bar{A}^{-1} L^{(k+2)} \end{aligned} \quad (\text{A11})$$

allows us to construct the expansion coefficients $f^{(k)}$ by induction of eq. (A11). The first three reduce to

$$\bar{f}_i^{(0)} = f_i^{(eq,0)}(\phi^{(0)}), \quad (\text{A12})$$

$$\bar{f}_i^{(1)} = f_i^{(eq,0)}(\phi^{(1)}) + f_i^{(eq,1)}(\phi^{(0)}, \mathbf{u}^{(1)}) - \bar{A}^{-1} (\boldsymbol{\xi}_i \cdot \boldsymbol{\nabla}) \bar{f}_i^{(0)}, \quad (\text{A13})$$

$$\begin{aligned} \bar{f}_i^{(2)} = & f_i^{(eq,0)}(\phi^{(2)}) + f_i^{(eq,1)}(\phi^{(0)}, \mathbf{u}^{(2)}) + f_i^{(eq,1)}(\phi^{(1)}, \mathbf{u}^{(1)}) + f_i^{(eq,2)}(\phi^{(0)}, \mathbf{u}^{(1)}, \mathbf{u}^{(1)}) \\ & - \bar{A}^{-1} \left[(\boldsymbol{\xi}_i \cdot \boldsymbol{\nabla}) \bar{f}_i^{(1)} + \left(\partial_t + \frac{1}{2} (\boldsymbol{\xi}_i \cdot \boldsymbol{\nabla})^2 \right) \bar{f}_i^{(0)} \right]. \end{aligned} \quad (\text{A14})$$

Introducing now the j-th moment over $\bar{f}^{(k)}$, $L^{(k)}$ and $F^{(k)}$ by $\mathcal{M}_j^{(k)}$, $\mathcal{L}_j^{(k)}$ and $\mathcal{F}_j^{(k)}$ and writing down the relevant contributions in more detail

$$\mathcal{M}_0^{(0)} = \phi^{(0)}, \quad \mathcal{M}_0^{(1)} = \phi^{(1)}, \quad \mathcal{M}_0^{(2)} = \phi^{(2)} - \bar{A}^{-1} [\boldsymbol{\nabla} \cdot (\phi^{(0)} \mathbf{u}^{(1)}) + \boldsymbol{\nabla}^2 P^{(0)} / 2 + \partial_t \phi^{(0)}], \quad (\text{A15})$$

$$\mathcal{M}_1^{(0)} = \phi^{(0)} \mathbf{u}^{(0)} = 0, \quad \mathcal{M}_1^{(1)} = \phi^{(0)} \mathbf{u}^{(1)}, \quad \mathcal{M}_1^{(2)} = \phi^{(1)} \mathbf{u}^{(1)} + \phi^{(0)} \mathbf{u}^{(2)} - \bar{A}^{-1} [\boldsymbol{\nabla} P^{(1)}], \quad (\text{A16})$$

$$\mathcal{M}_2^{(0)} = P^{(0)} \mathbf{I}, \quad \mathcal{M}_2^{(1)} = P^{(1)} \mathbf{I}, \quad \mathcal{M}_2^{(2)} = P^{(2)} \mathbf{I} + \phi^{(0)} \mathbf{u}^{(1)} \mathbf{u}^{(1)} - \bar{A}^{-1} \mathcal{D}^{(1)} \quad (\text{A17})$$

and

$$\mathcal{F}_0^{(3)} = \phi^{(0)} s^{(1)} \quad \mathcal{F}_1^{(3)} = \phi^{(0)} \mathbf{a}^{(1)} \quad \mathcal{F}_2^{(3)} = \frac{dP^{(0)}}{d\phi^{(0)}} \phi^{(0)} s^{(1)} \mathbf{I} \quad (\text{A18})$$

$$\mathcal{L}_0^{(3)} = \bar{\lambda} \mathcal{F}_0^{(3)} \quad \mathcal{L}_1^{(3)} = \bar{\lambda} \mathcal{F}_1^{(3)} - \mathcal{C}_1^{(3)} \quad \mathcal{L}_2^{(3)} = \bar{\lambda} \mathcal{F}_2^{(3)} \quad (\text{A19})$$

with the barotropic pressure terms up to $\mathcal{O}(\epsilon^2)$

$$P^{(0)} = \frac{1}{2\kappa_n^2}(\phi^{(0)})^2 \quad P^{(1)} = \frac{1}{\kappa_n^2}\phi^{(0)}\phi^{(1)} \quad P^{(2)} = \frac{1}{2\kappa_n^2}(2\phi^{(0)}\phi^{(2)} + (\phi^{(1)})^2) \quad (\text{A20})$$

and the dissipative and residual term for $k = 1$

$$\nabla \cdot \mathcal{D}^{(1)} = \sum_{i=0}^8 \xi_i (\xi_i \cdot \nabla)^2 f^{(1)} = \theta [\nabla^2 (\phi^{(0)} \mathbf{u}^{(1)}) + 2\nabla (\nabla \cdot (\phi^{(0)} \mathbf{u}^{(1)}))] \quad (\text{A21})$$

$$\mathcal{C}_1^{(3)} = \sum_{i=0}^8 \xi_i (\xi_i \cdot \nabla) [\partial_t + (\xi_i \cdot \nabla)^2 / 6] \bar{f}_i^{(0)} \quad (\text{A22})$$

Taking the zeroth and first moment over eq. (A8) yields

$$\partial_t \mathcal{M}_0^{(k)} + \nabla \cdot \mathcal{M}_1^{(k+1)} + \frac{1}{2} \nabla \nabla : \mathcal{M}_2^{(k)} = \mathcal{L}_0^{(k+2)} \quad (\text{A23})$$

$$\partial_t \mathcal{M}_1^{(k)} + \nabla \cdot \mathcal{M}_2^{(k+1)} + \frac{1}{2} \nabla \cdot \mathcal{D}^{(k)} = \mathcal{L}_1^{(k+2)} \quad (\text{A24})$$

For $k = -1$ eq. (A24) delivers following constraint for the pressure $\nabla P^{(0)} = 0$, allowing us to choose $\phi^{(0)} = 1$ due to $\phi^{(0)} \nabla \phi^{(0)} = 0$ resulting in $\mathbf{u}^{(0)} = 0$. For $k = 0$ eq. (A23) reduces to

$$\partial_t \phi^{(0)} + \nabla \cdot \phi^{(0)} \mathbf{u}^{(1)} = 0 \quad (\text{A25})$$

whereas eq. (A24) yields $\nabla P^{(1)} = 0$, which permits us to choose $\phi^{(1)} = 0$ due to $\phi^{(1)} \nabla \phi^{(0)} + \phi^{(0)} \nabla \phi^{(1)} = 0$. As a consequence the pressure terms up to $\mathcal{O}(\epsilon^3)$ are fixed to $P^{(0)} = 1/(\kappa_n^2)$, $P^{(1)} = 0$, $P^{(2)} = 1/(\kappa_n^2)\phi^{(2)}$ and $P^{(3)} = 1/(\kappa_n^2)\phi^{(3)}$. From eq. (A25) the incompressibility condition for $\mathbf{u}^{(1)}$ follows immediately

$$\nabla \cdot \mathbf{u}^{(1)} = 0. \quad (\text{A26})$$

Applying these properties for eqs. (A23) and (A24) for $k = 1$ results in

$$\partial_t \phi^{(1)} + \nabla \cdot [\phi^{(1)} \mathbf{u}^{(1)} + \phi^{(0)} \mathbf{u}^{(2)}] = \bar{\lambda} \phi^{(0)} s^{(1)}, \quad (\text{A27})$$

$$\partial_t \phi^{(0)} \mathbf{u}^{(1)} + \nabla \cdot [\phi^{(0)} \mathbf{u}^{(1)} \mathbf{u}^{(1)} + P^{(2)} \mathbf{I}] + \left(\frac{1}{2} - \frac{1}{A} \right) \nabla \cdot \mathcal{D}^{(1)} = \bar{\lambda} \phi^{(0)} \mathbf{a}^{(1)} - \mathcal{C}_1^{(3)} \quad (\text{A28})$$

Substituting the constraints for $\phi^{(0)} = 1$ and $\phi^{(1)} = 0$ into the latter two equations we obtain compressibility effects at $\mathcal{O}(\epsilon^2)$ due to the intrinsic source term. Additionally the residual term on the right hand side of eq. A28 vanishes

$$\nabla \cdot \mathbf{u}^{(2)} = \bar{\lambda} s^{(1)}, \quad (\text{A29})$$

$$\partial_t \mathbf{u}^{(1)} + \nabla \cdot (\mathbf{u}^{(1)} \mathbf{u}^{(1)}) + \frac{1}{\kappa_n^2} \nabla \phi^{(2)} + \theta \left(\frac{1}{2} - \frac{1}{A} \right) \nabla^2 \mathbf{u}^{(1)} = \bar{\lambda} \mathbf{a}^{(1)}. \quad (\text{A30})$$

For $k = 2$ for eqs. (A23) and (A24) the derivation gives

$$\partial_t \phi^{(2)} + \nabla \cdot [\phi^{(2)} \mathbf{u}^{(1)} + \phi^{(0)} \mathbf{u}^{(3)}] = \bar{\lambda} \phi^{(0)} s^{(2)}, \quad (\text{A31})$$

$$\partial_t \phi^{(0)} \mathbf{u}^{(2)} + \nabla \cdot [\phi^{(0)} (\mathbf{u}^{(1)} \mathbf{u}^{(2)} + \mathbf{u}^{(2)} \mathbf{u}^{(1)}) + P^{(3)} \mathbf{I}] + \left(\frac{1}{2} - \frac{1}{A} \right) \nabla \cdot \mathcal{D}^{(2)} = \bar{\lambda} \phi^{(0)} \mathbf{a}^{(2)} - \mathcal{C}_1^{(4)}, \quad (\text{A32})$$

which reduces analogously to

$$\partial_t \phi^{(2)} + \mathbf{u}^{(1)} \cdot \nabla \phi^{(2)} + \nabla \cdot \mathbf{u}^{(3)} = \bar{\lambda} s^{(2)}, \quad (\text{A33})$$

$$\partial_t \mathbf{u}^{(2)} + \nabla \cdot (\mathbf{u}^{(1)} \mathbf{u}^{(2)} + \mathbf{u}^{(2)} \mathbf{u}^{(1)}) + \frac{1}{\kappa_n^2} \nabla \phi^{(3)} + \theta \left(\frac{1}{2} - \frac{1}{A} \right) [\nabla^2 \mathbf{u}^{(2)} + 2 \nabla (\nabla \cdot \mathbf{u}^{(2)})] = \bar{\lambda} \mathbf{a}^{(2)}. \quad (\text{A34})$$

To show the deviations from the anticipated model equations (2) and (3) at $\mathcal{O}(\epsilon^3)$ we multiply eq. (A26) with ϵ , eq. (A29) with ϵ^2 , eq. (A33) with ϵ^3 , eq. (A30) with ϵ^2 and eq. (A34) with ϵ^3 . Summing them up and introducing quantities up to order $\mathcal{O}(\epsilon^3)$

$$\tilde{\phi} = 1 + \epsilon^2 \phi^{(2)}, \quad \tilde{\mathbf{u}} = \epsilon \mathbf{u}^{(1)} + \epsilon^2 \mathbf{u}^{(2)} \quad \tilde{P} = \epsilon^2 P^{(2)} + \epsilon^3 P^{(3)}, \quad (\text{A35})$$

$$\tilde{s} = \epsilon s^{(1)} + \epsilon^2 s^{(2)} = \kappa_n (\epsilon u_x^{(1)} + \epsilon^2 u_x^{(2)}), \quad \tilde{\mathbf{a}} = \epsilon \mathbf{a}^{(1)} + \epsilon^2 \mathbf{a}^{(2)} = \kappa_n^{-1} (\epsilon \mathbf{u}^{(1)} + \epsilon^2 \mathbf{u}^{(2)}) \times \mathbf{e}_z + \epsilon^2 \mathbf{u}^{(1)} s^{(1)} \quad (\text{A36})$$

yields with the viscosity modification $\tilde{\nu} = \theta (1/A - 1/2)$ and the operator $d_t^{(1)} = \partial_t + \mathbf{u}^{(1)} \cdot \nabla$

$$\epsilon \frac{d^{(1)}}{dt} \tilde{\phi} + \epsilon^3 \nabla \cdot \mathbf{u}^{(3)} + \nabla \cdot \tilde{\mathbf{u}} = \epsilon \bar{\lambda} \kappa_n \tilde{u}_x + \mathcal{O}(\epsilon^4), \quad (\text{A37})$$

$$\epsilon \frac{d^{(1)}}{dt} \tilde{\mathbf{u}} + \epsilon^3 \mathbf{u}^{(2)} \cdot \nabla \mathbf{u}^{(1)} + \epsilon \bar{\lambda} \kappa_n^{-1} \mathbf{e}_z \times \tilde{\mathbf{u}} = -\nabla \tilde{P} + \epsilon \tilde{\nu} [\nabla^2 \tilde{\mathbf{u}} + 2 \nabla (\nabla \cdot \epsilon^2 \mathbf{u}^{(2)})] + \mathcal{O}(\epsilon^4). \quad (\text{A38})$$

In eq. (A38) the source term appearing in $\mathbf{a}^{(2)}$ cancels an additional term arising from the advective derivative term at $\mathcal{O}(\epsilon^3)$. The result shows that the approximation to the magnetised plasma equations (2) and (3) are at least second order accurate and that the deviations from this set appear at $\mathcal{O}(\epsilon^3)$. As a consequence of the diffusive scaling this refers to second-order accuracy in space and first-order accuracy in time. Moreover the Newtonian deviatoric stress $\boldsymbol{\sigma}'_N = \tilde{\nu} \tilde{\phi} [(\nabla \tilde{\mathbf{u}}) + (\nabla \tilde{\mathbf{u}})^T - \frac{1}{2} (\nabla \cdot \tilde{\mathbf{u}}) \mathbf{I}] + \zeta \tilde{\phi} (\nabla \cdot \tilde{\mathbf{u}}) \mathbf{I}$ appears with an artificial bulk viscosity $\zeta = (5/3) \tilde{\nu}$ at $\mathcal{O}(\epsilon^4)^6$.

REFERENCES

- ¹S. Chen, H. Chen, D. Martinez and W. Matthaeus, Phys. Rev. Lett. 67, 37763779 (1991).
- ²S. Succi, M. Vergassola, R. Benzi, Phys. Rev. A 43, 45214524 (1991)
- ³D.O. Martinez, S. Chen, W.H. Matthaeus, Phys. Plasmas 1, 1850 (1994).
- ⁴L. Vahala, D. Wah, G. Vahala, J. Carter, P. Pavlo, Physical Review E **62**, 507 (2000).
- ⁵W. Schaffnerberger, A. Hanselmeier, Phys. Rev. E 66, 046702 (2002)
- ⁶P.J. Dellar, Phys. Rev. E, 65, 036309 (2002).
- ⁷P.J. Dellar J. Comput. Phys., 190, 351370 (2003).
- ⁸G. Breyiannis, D. Valougeorgis, Phys. Rev. E 69, 065702(R) (2004).
- ⁹A. Macnab, G. Vahala, L. Vahala, J. Carter, M. Soe and W. Dorland, Physica A **362**, 48 (2006).
- ¹⁰G. Vahala, B. Keating, M. Soe, J. Yepez, L. Vahala, J. Carter et al. Commun. Comput. Phys., 4 (2008), pp. 624646
- ¹¹M. Pattison, K. Premnath, N. Morley, M. Abdou, Fusion Eng. Design, 83, 557 (2008).
- ¹²J. Statist. Mech. P06003 (2009).
- ¹³D. Chatterjee and S. Amiroudine, Phys. Rev. E 81, 066703 (2010)
- ¹⁴P.J. Dellar, Computers & Fluids 46, 201 (2011)
- ¹⁵P.J. Dellar, Journal of Computational Physics 237, 115 (2013).
- ¹⁶P.J. Dellar, J. Comput. Phys. 179, 05 (2002).
- ¹⁷M. Mendoza and J. D. Munoz, Phys. Rev. E **77**, 026713 (2008).
- ¹⁸G. Fogaccia, R. Benzi and F. Romanelli, Phys. Rev. E **54** 4384, (1996).
- ¹⁹A. Hasegawa, K. Mima, Physical Review Letters 4, 205 (1977).
- ²⁰J.G. Charney, Geophys. Publ. Oslo 17, 1 (1948).
- ²¹A. Kendl, Eur. J. Phys. 29, 911-926 (2008).
- ²²B. D. Scott, Plasma Phys. Control. Fusion 49, S25-41 (2007).
- ²³J. A. Krommes, Annu. Rev. Fluid. Mech. 44, 175-201 (2012).
- ²⁴W. Horton and A. Hasegawa, Chaos 4, 227 (1994).
- ²⁵L. H. Zhong, S. D. Feng, S. T. Gao Adv. Atmos. Sci. 22, 349-358 (2005).
- ²⁶L. Zhong, S. D. Feng, S. T. Gao Advances atmos . Sci 23, 561-578 (2006).
- ²⁷L. H. Zhong, S. D. Feng, S. T. Gao Chinese J. Geophysics-Chinese Edition 49, 1257-1270 (2006).

- ²⁸P. J. Dellar, <http://www.serc.iisc.ernet.in/~raha/onGELatticeBoltzmannProblem.pdf> (2000), (last accessed on 27.05.2014) .
- ²⁹P. L. Bhatnagar, E. P. Gross, M. Krook, Phys. Rev. 94, 511-525 (1954).
- ³⁰R. Salmon, Journal of Marine Research 3, 503-535 (1999)
- ³¹L.-S. Luo, Phys. Rev. Lett. 81, 1618 - 1621 (1998)
- ³²P.J. Dellar, Computers & Mathematics with Applications 65, 129 (2013)
- ³³S. Succi, *The Lattice Boltzmann Equation for Fluid Dynamics and Beyond*. Oxford University Press, 2001.
- ³⁴V. Naulin and A.H. Nielsen, SIAM J. Sci. Comput. 25, 104 (2003).
- ³⁵A. Arakawa, Journal of Computational Physics 1, 119 (1966).
- ³⁶G.E. Karniadakis, S.A. Orszag, and M. Israeli, Journal of Computational Physics 97, 414 (1991).
- ³⁷V. Naulin, New Journal of Physics 4, 28 (2002).
- ³⁸C.F. Fontán and A. Varga, Physical Review E 6, 6717 (1995).
- ³⁹M. Kono and M. Skoric, *Nonlinear Physics of Plasmas*. Springer, 2010.
- ⁴⁰K. Iga and T. Watanabe, Journal of the Meteorological Society of Japan 5, 895 (2003).
- ⁴¹V.D. Larichev and J.C. McWilliams, Phys. Fluids A 5, 938 (1991).
- ⁴²G. Manfredi, Journal of Plasma Physics 4, 601 (1999).
- ⁴³F.J. Harris, Proceedings of the IEEE 66, 51 (1978).
- ⁴⁴M. Ottaviani and J.A. Krommes, Physical Review Letters 69, 2923 (1992).
- ⁴⁵N. Kukharkin, S.A. Orszag and V. Yakhot, Physical Review Letters 13, 2486 (1995).
- ⁴⁶P.J. Dellar, Journal of Differential Equations 176, 29 (2001).
- ⁴⁷X. He, S. Chen, G. D. Doolen, J. Comput. Phys. 146, 282-300 (1998).
- ⁴⁸R. Salmon, J. Marine Res. 57, 847-884 (1999).
- ⁴⁹H. Yu, S.S.. Girimaji, L.-S. Luo , J. Comput. Phys. 209, 599-616 (2005).
- ⁵⁰M. Tsutahara, M. Okabayashi, T. Kataoka, Computational Fluid Dynamics 2000 (ed N. Satofuka), pp. 529-544 (2001).
- ⁵¹Y. Sone, Boston: Birkhäuser (2002).
- ⁵²M. Junk, A. Klar, L.S. Luo, J. Comput. Phys. 210, 676-704 (2005).
- ⁵³M. Junk, W.-A. Yong, Asymptotic Analysis 35, 165-185 (2003).
- ⁵⁴T. Inamuro, M. Yoshino, F. Ogino, Phys. Fluids 9, 3535-3542, (1997).
- ⁵⁵P. Asinari, Computers and mathematics with Applications 55, 1392-1407 (2008).